*Korean J. Chem. Eng.*, 39(8), 2217-2228 (2022)
DOI: 10.1007/s11814-022-1069-4

pISSN: 0256-1115
eISSN: 1975-7220

# The removal of Cr(VI) from aqueous and saturated porous media by nanoscale zero-valent iron stabilized with flaxseed gum extract: Synthesis by continuous flow injection method

**Neman Izadi, Banafsheh Haji Ali, Mohammad Sajjad Shahin, and Majid Baghdadi†**

School of Environment, College of Engineering, University of Tehran, Tehran, Iran
(*Received 30 November 2021 • Revised 13 January 2022 • Accepted 17 January 2022*)

**Abstract**−Recently, the in-situ removal of contaminants by iron nanoparticles has been considered due to their non-toxicity, abundance, ease of production, and cost-effectiveness, which can be accomplished by injecting them underground. In this study, nZVI was synthesized using a novel continuous synthesis method using flaxseed glaze as a green, non-toxic, and low-priced coating. The produced nanoparticles were characterized by dynamic diffraction analysis (DLS), field electron microscopy (FE-SEM), X-ray spectroscopy (EDX), and infrared spectroscopy (FTIR) spectroscopy. Batch experiments were conducted to evaluate the effect of Cr(VI) concentration, FG-nZVI dosage, pH, and coexisting components (Total dissolved solids, Humic acid, and $NO_3^-$) on Cr(VI) removal. Results of the characterization and identification, and stability tests indicated that nanoparticles synthesized by using this continuous synthesis system were smaller and more regular shaped than those prepared by conventional synthesis. According to the results, the Cr(VI) residual level increased by increasing the initial Cr(VI) concentration and decreased by increasing the nZVI coated with flaxseed glaze (FG-nZVI) dosage. At the Cr(VI) initial concentration of 4 mg $L^{-1}$, the Cr(VI) was removed entirely at almost all dosages of FG-nZVI. Optimal amount of FG-nZVI was 62.73 mg $L^{-1}$ when applied at 4 mg $L^{-1}$ of Cr(VI) at optimum pH 6.64, resulting in the Cr(VI) residual concentration of 0.05 mg $L^{-1}$. The results of saturated porous media showed that injection background solutions enhanced the transfer of nanoparticles in the porous medium, resulting in the adequate removal along the desired radius. The results illustrated that using FG-nZVI can be effective for practical groundwater remediation.

Keywords: Cr(VI) Removal, Flaxseed Gum, Green Synthesis, Continuous Synthesis System, nZVI Stabilization

## INTRODUCTION

Among toxic heavy metals, chromium is used in various industrial processes such as stainless steel, pigment production, tanning and leather, metal plating, crude oil refinery, and wood preservatives [1-3]. Metal chromium is usually found in industrial waste sites from the leather industry, electroplating, and other industries. Various forms of chromium pollution have been observed in surface water, soil, and groundwater [4-9]. Two common forms of chromium in aqueous environments are hexavalent chromium (Cr(VI)) and trivalent chromium (Cr(III)). Cr(VI) is more mobile, soluble, and toxic than Cr(III), and in addition, the World Health Organization considers Cr(VI) as human mutagen and carcinogen [10]. According to the hazard posed by Cr(VI), it is crucial to find efficient methods for removing Cr(VI) from aqueous environments. Most methods used to treat contaminated environments involve chemical precipitation, coagulation, bioreduction, adsorption, electrolysis, membrane separation and photocatalysis. The most prevalent method of chromium pollution control is the conversion of Cr(VI) to Cr(III) [11,12].

To treat contaminated groundwater, various methods have been used, including pump and treat (P&T), the permeable reactive barriers (PRBs), and direct injection into the aquifer. Nevertheless, these methods have many limitations, such as high costs, the need for bulky drilling, unsuitability for deep aquifers, and the requirement for PRBs against pollution [13]. Considering the difficulty of treating contaminants in groundwater, direct injection of materials into the aquifer has been considered as a suitable alternative for decontaminating groundwater. In fact, injection of reactive materials directly into aquifers offers many advantages, including a lower cost than other methods, the ease of creating a reactive zone without heavy drilling, and the ability to inject directly into contaminated areas and deep aquifers [14].

In the past decade, there have been several biomaterials such as carboxylate graphene oxide, polydopamine, biometallohydrogel which have been used as a coating for nanoparticles [15-17]. Nanoscale zero valent iron has emerged as an attractive option for treating organic and inorganic contaminants in soil and aqueous solutions because of its being environmentally friendly, cost-effective, with large specific surface area and high reduction capacity [18,19]. According to prior research, nZVI can be applied to effectively remove Cr(VI) from contaminated soil and aqueous solutions [20]. The interaction mechanism of Cr(VI) by nZVI is mainly attributed to the reduction of Cr(VI) to Cr(III). Thus, during the process of reduction, the possible reactions are as follows: Eq. (1) and (2) [21]:

$$2HCrO_4^- + 3Fe^0 + 14H^+ \rightarrow 3Fe^{2+} + 2Cr^{3+} + 8H_2O \quad (1)$$

†To whom correspondence should be addressed.
E-mail: m.baghdadi@ut.ac.ir
Copyright by The Korean Institute of Chemical Engineers.

$$Cr_2O_7^{2-}+6Fe^{2+}+14H^+\rightarrow 6Fe^{3+}+2Cr^{3+}+7H_2O \quad (2)$$

However, previous studies have shown that the oxide shell, which is created by the reaction of dissolved oxygen (DO) or water with nZVI particles, can easily cover exposed nZVI particles, resulting in their passivation and inactivation [22,23]. Additionally, nZVIs tend to aggregate rapidly because of magnetic and chemical interactions [24]. These factors cause the loss of specific surface area and high reactivity of nanoparticles, thereby limiting their use [25,26]. Also, the transfer of bare nanoparticles to the saturated porous medium due to its rapid deposition at the injection site and improper distribution in the polluted area will cause clogging of cavities [27]. To overcome the limitations of nZVI, extensive research has been conducted over the past decade to modify and stabilize nZVIs. In general, the modification techniques of nZVI include surface coatings, solid supports, and doped metals (which include Ni, Cu, Pd, Pt, Ag and Au) [28-30]. In fact, surface coatings on nanoparticles not only can prevent the nanoparticles from coming close to each other but also deal with the magnetic attraction between them owing to changing the surface charge of the iron particles, which helps to keep them stable [14]. Various materials such as polymers (such as Amphiphilic polysiloxane graft copolymers (APGCs)), Olefin-maleic acid copolymer and Polyacrylic acid (PAA)), biopolymers (such as Carboxymethyl cellulose, starch, alginate, guar gum, xanthan gum), and ionic and nonionic surfactants (such as Tween 85 and sodium dodecyl sulfate (SDS)) have been proposed as surface coatings for iron nanoparticles [31-38]. However, it is important to find a suitable modification strategy because not all the materials mentioned affect nZVI positively.

In general, the extract of plants is biocompatible, harmless, economical, and energy-efficient, making them ideal for coating the surface of the iron particles. Relevant studies demonstrate several green substances as a stabilizer, which have been employed to prepare stable iron nanoparticles. An example is guar gum, a biodegradable nontoxic green polymer polysaccharide which leads to synthesize nanoparticles from 500 nm to less than 200 nm and prevents their aggregation [39]. Results obtained by Wang et al. [40] indicated that using carboxymethyl cellulose as a stabilizer for iron nanoparticles led to less agglomeration, but the significant decrease in Cr(VI) reduced power as compared to ones synthesized without a stabilizer. In another study by Dong et al. [34], polyacrylic acid and starch were implemented as a stabilizer in the preparation of iron nanoparticles. The authors concluded that coating the nanoparticle surface increased chromium removal by increasing the active surfaces for the reaction, but too much coating decreased iron nanoparticle reactivity. However, this is the first time that nZVIs have been modified with flaxseed glaze and no studies have investigated the effect of coated flaxseed glaze on nanoscale zero-valent iron particles on Cr(VI) removal for water remediation. In this study, flaxseed glaze - a low cost, widespread, environmentally friendly and green (natural) material - has been successfully used as an effective coating and stabilizer in the preparation of iron nanoparticles. Flaxseed is usually used in the food and pharmaceutical industries. In fact, flaxseed glaze, which interacts with nZVI and covers their surfaces, makes iron nanoparticles much more stable, so that nZVIs are separated from each other and dispersed better.

For the synthesis of nZVI, various physical and chemical methods have been used, such as grinding, abrasion, lithography, nucleation from homogeneous solutions or gasses, annealing at elevated temperatures, and reacting with reducing agents, which are categorized under two main methods: the bottom-up and top-down approaches [39,41]. The borohydride reduction of ferrous salts is one of the most popular chemical synthesis methods because it is simple, requiring no special instruments or materials. Although the borohydride reduction of ferrous salts is one of the most popular chemical synthesis methods because of its simplicity as no special instruments or materials are required, it is batch synthesis that needs a long time to conduct chemical reactions and produce homogeneous nanoparticles [39]. In this study, for the first time, a continuous synthesis system is applied to the chemical synthesis process of nZVI. By using the liquid-phase reduction method to continuously synthesize nZVI, less environmentally harmful materials are used, and highly reactive nanoparticles can be produced with excellent chemical homogeneity.

In this study, nanoscale zero-valent iron was prepared by green synthesis for the first time as a natural material using flaxseed gum. The continuous flow injection system was used as a novel method, which made great stability in comparison with conventional injection. In general, the primary objective of this study was to synthesize flaxseed glaze-stabilized nZVI (FG-nZVI) by using the novel continuous synthesis system. The specific aim was to investigate the performance for the removal of Cr(VI) by FG -nZVI from the aqueous solution and the saturated porous medium.

## MATERIAL AND METHODS

### 1. Materials and Instruments

In this study, ferrous sulfate ($FeSO_4{\cdot}7H_2O$), sodium borohydride ($NaBH_4$), and starch were used for the preparation of nanoscale zero-valent iron (nZVI). The pH was adjusted by using sodium hydroxide (NaOH) and hydrochloric acid (HCl). Moreover, simulated groundwater was prepared by adding $CaCl_2$, $MgSO_4{\cdot}7H_2O$, $NaHCO_3$, and $KNO_3$ in deionized water. Also, potassium dichromate ($K_2Cr_2O_7$) was utilized to prepare Cr(VI) solution. All chemicals applied in this study were of reagent grade purchased from Merck Co., while flaxseed and carboxymethyl cellulose (CMC) were obtained from an Iranian traditional herbal shop (Attari). All tests to evaluate the stability of nZVI in an aqueous suspension were performed at pH 7.5. In addition, purified $N_2$ gas, purchased from ROHAM GAS Co (Iran), was used to remove dissolved oxygen from deionized water. The residual Cr(VI) solution concentration was determined using a spectrophotometer (Hach-DR5000) at a wavelength of 540 nm by the diphenylcarbazide method, and a chromotropic acid method was used for the direct detection of nitrate in solutions.

### 2. Preparation of Coating Reagent (Flaxseed Glaze)

The flaxseed glaze was prepared as follows: after cleaning and removing impurities of flaxseed, 2 gr of flaxseed was added to 250 mL of the deionized water. Then, the mixture was heated to raise its temperature to the boiling point and boiled until 50 mL of water was evaporated. The resultant liquid containing flaxseed glaze was used as a coating for nZVI in this research. 0.2 gr of glaze was ex-

tracted from each gram of flaxseed.

**3. Nanoparticle Preparation via Continuous Production Method**

For synthesizing 0.10 g of nZVI, a 100 mL flask was filled with 0.498 g of $FeSO_4 \cdot 7H_2O$ and 80 mL of produced gum solution containing 0.19 g of gum afterward and then diluted to volume with deoxygenated deionized water. A magnetic stirrer was used to stir the solution for 15 min until a homogeneous Fe-FS complex was created. To prepare the reducing agent, 0.135 g of $NaBH_4$ was dissolved in 100 mL of deoxygenated deionized water.

A peristaltic pump (A) was used to pump a ferrous salt dissolved in flaxseed gum from an injection syringe to the reaction vessel. The sodium borohydride was injected from an injection syringe to the reaction zone using a high-pressure peristaltic pump (B) in the following part. The third section's reaction zone is separated from the sodium borohydride injection zone but close to the spiral reaction pipe. A spiral pipe with a length of 25 cm and nine spiral rings was installed to mix the flow together well in the tube to complete the synthesis reaction process. Following the ejection, the nanoparticles were released (Fig. S1).

According to the experiments, the optimal model was found, which indicated that flaxseed gum is suitable for stabilization. Besides, the desired amount of coating (coating/Fe) was investigated at the Cr(VI) concentration of 10 mg $L^{-1}$, FG-nZVI dosage of 3 mg, pH of 7.0, and the reaction time of 40 min to achieve the best performance. The effect of different Fe concentration with a constant coating concentration of 0.80 $gL^{-1}$ was also analyzed, and it was found that 0.50 $gL^{-1}$ had the best stability. Besides, nanoparticles become more stable as the flow rate increases from 1.5-5-10-15 $mLmin^{-1}$. Moreover, the most remarkable results were obtained using synthesized nanoparticles in a continuous injection procedure with a fine-diameter needle.

**4. The Characterization**

The synthesized nZVI particles' morphology and size were assessed by field emission scanning electron microscopes (FE-SEM; MIRA3 TESCAN-XMU). The nanoparticle solution was passed through a syringe filter with a 200 nm pore size to prevent nanoparticle oxidation and accumulation. After the filter saturation with nanoparticles, it was washed with methanol and dried by $N_2$ gas blowdown. Also, to prevent corrosion, the sample was sealed. Dynamic light scattering (DLS, Zetasizer Nano ZS MALVERN) was used to determine the size distribution profile of particles and the zeta potential. Before DLS synthesis, the nanoparticle sample was placed in an ultrasonic bath (Model 300, Pulse, Italy) for 5 min. The elemental composition of the flaxseed glaze was determined with the CHNS analyzer (Elementar Analysensysteme, Hanau, Germany). A Fourier transform infrared (FTIR, Bruker Tensor 27, Germany) was used to record FTIR spectra of samples.

**5. Porous Media**

To investigate the removal of Cr(VI) in saturated porous media, silica sand was used as a porous media. The prepared sand was initially sieved to attain the size range of 0.354 to 420 mm. The used sieve size was from #40 (425 mm openings) to #45 (355 mm openings). Then it was washed three times by dilute hydrochloric acid (HCl 0.1 mol $L^{-1}$) to remove impurities. According to Eq. (3) and (4), the pore volume of the sand was calculated as follows [42]:

$$\varepsilon = \frac{V_p}{V_t} \times 100 \tag{3}$$

$$V_{PV} = \varepsilon \times V \tag{4}$$

where, $\varepsilon$ is the porosity of samples; $V_p$ is the pore volume of samples filled with water, $cm^3$; $V_t$ is the total of samples filled with sand and water, $cm^3$; $V_{PV}$ is the total pore volume of sand, $cm^3$; V is the total volume of samples, $cm^3$.

**6. Batch Experiments for Cr (VI) Removal**

All batch experiments for removing Cr(VI) ions from aqueous solutions were conducted in 100 mL at room temperature (23 °C). The Cr(VI) stock solution was diluted to produce various initial concentrations of Cr(VI). After the reaction time, aeration by the aquarium pump was used to settle the dissolved iron in the solution after all experiments. The appropriate mass ratio of coating/Fe was investigated. The pH of prepared solutions was adjusted by adding dilute hydrochloric acid (HCl, 0.1 mol $L^{-1}$) or sodium hydroxide (NaOH, 0.1 mol $L^{-1}$) and using a pH meter (model 690, Metrohm). In addition, FG-nZVI was studied in relation to water chemistry (TDS, $NO_3^-$ and HA). Each experiment was done three times and the average was reported as a result.

**7. The Design and Analysis of Batch Experiments for Cr(VI) Removal**

Box-Behnken design (BBD) was applied to optimize the influential factors involved in the experiments. To define effective parameters on the removal of Cr(VI) and the range of selected parameters, preliminary experiments were carried out. Three independent variables, initial Cr(VI) concentration, FG-nZVI dosages, and pH, were chosen to study in the current research and marked A, B, and C, respectively. Table S1 indicates the value of the chosen variables. Eq. (5) is used to calculate the required number of experimental runs, where K is the number of the factors studied in the experiments, and $C_0$ is the number of central points. Hence, in this study, the total run number was 17 following the Box-Behnken design (BBD) based on a three-level factors design with five central points.

$$N = 2K(K-1) + C_0 \tag{5}$$

Design-Expert software (Version 10) was used to design and analyze experiments. The related design matrix design is given in Table S4 Analysis of variance (ANOVA), a statistical technique applied to check the model validity and the correlation between the model and the actual observed data. Moreover, the $R^2$ statistic (coefficient of determination) and the adjusted R-squared were used to evaluate the model fitness.

**8. The Removal Cr(VI) in the Saturated Porous Medium**

The experiments for removing Cr(VI) from saturated porous media were performed in a laboratory-scale column packed with sand under saturated conditions. A polyethylene column with a 27 cm internal diameter was filled with silica sands up to a length of 7 cm. Then, the porous media was saturated with Cr(VI)-contaminated water (1.4 L) in two different concentrations (6.0 and 12 mg $L^{-1}$). The saturated porous medium measured porosity and pore volume were, respectively, 0.41 and 16.53 L. In this study, the direct injection of reactive media under pressure was used as an injection method. The design parameters of direct injection included the following: injection spacing (the horizontal distance between injec-

tion points), injection interval (the vertical distance between injections over the injection thickness), injection pressure (whether to utilize a lower pressure to spread through an impenetrable layer with the reactive media or a higher pressure to break a permeable layer of soil), and injection "chase water" to increase the distribution of reactive media [43]. In the experiments, two different dosages of FG-nZVI (0.05 and 0.075 g) were injected directly downward into the center of the sand column by using a peristaltic pump (Ismatec, Germany). To study the mobility of dispersed FG-nZVI in the saturated porous medium and its influence on the removal Cr(VI), 200 mL of the background solution was injected at three different flow rates (0, 30, and 60 $mLmin^{-1}$) into the same injection point of FG-nZVI in the saturated porous medium. Fig. S2 shows a schematic diagram of the utilized instruments and the experimental setup.

The samples were collected within different radii (4, 8, and 12 cm) and depths (2, 4, and 6 cm) at three various times (5, 20, and 60 min). Table S2 illustrates the five experiments that were performed under different conditions in this study. A spectrophotometric method was used to determine the Cr(VI) concentration.

## RESULTS AND DISCUSSION

### 1. The Characterization

The iron nanoparticles synthesized using the recommended flow injection system were analyzed by FESEM, DLS, EDX, CHNS, and FTIR. As observed from the FESEM and DLS images (Fig. 1(a)-(b)), most synthesized nZVI have regular spherical shapes and sizes less than 100 nm, showing optimal synthesis conditions preventing the aggregation of nanoparticles. The DLS image also shows that the nanoparticle size distribution is narrow and uniform. The EDX analysis of the nanoparticles presents that the surface of nanoparticles is mainly composed of iron. In addition, three peaks (C, O, and S) in Fig. 1(c) confirmed that nZVI particles were coated with the flaxseed glaze. This is consistent with the CHNS results (Table S3). According to the results of EDX analysis (Fig. 1(c)), the percentage of the elements of Fe, O, C, and S was determined to be 60.12, 17.44, 13.14, and 0.47, respectively. CHNS analysis was carried out to confirm the flaxseed glaze on the surface of nZVI (Table S3).

FTIR spectrometry is a valuable technique for determining the composition of molecules and multi-atom ions by investigating their vibrational peaks. Furthermore, since the spectra of organic compounds are highly complicated and have a broad range of maximum and maximum peaks, which could be used for comparison, this approach is often used for their detection. The wave number range was between 400 $cm^{-1}$ and 4,000 $cm^{-1}$. Fig. 1(d) illustrates that the broad peak between 3,400 $cm^{-1}$ and 3,500 $cm^{-1}$ was assigned to the stretching vibration of the hydroxyl groups (O-H) [44-46]. The sharp peak at 2,960 $cm^{-1}$ is ascribed to the stretching vibration of the C-H bond [47-50]. Another major peak is attributed to the N-H group, which is shown as 2,582 $cm^{-1}$ [49]. The additional peak at 2,349 $cm^{-1}$ corresponds to the stretching vibration of O=C=O bonds [4]. The rest of the minor peaks at 1,300 $cm^{-1}$ and 1,070 $cm^{-1}$ can be related to the S=O and C-O stretch of alcohol and carboxylic acids, respectively [51,52].

### 2. Stability and Aggregation of FG-nZVI

Sedimentation experiments were conducted to assess the stabil-

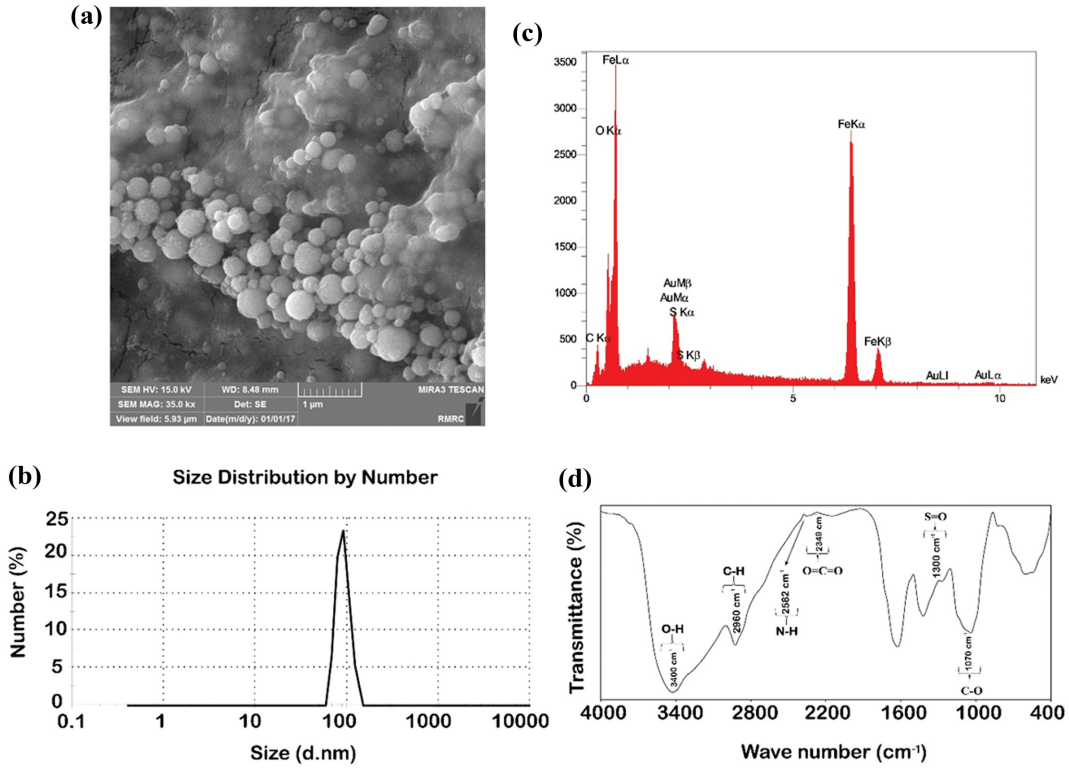



**Fig. 1. FE-SEM images of nZVI (a), DLS analysis of nZVI (b), EDS analysis of nZVI (c), and FTIR spectra for the flaxseed glaze (d).**

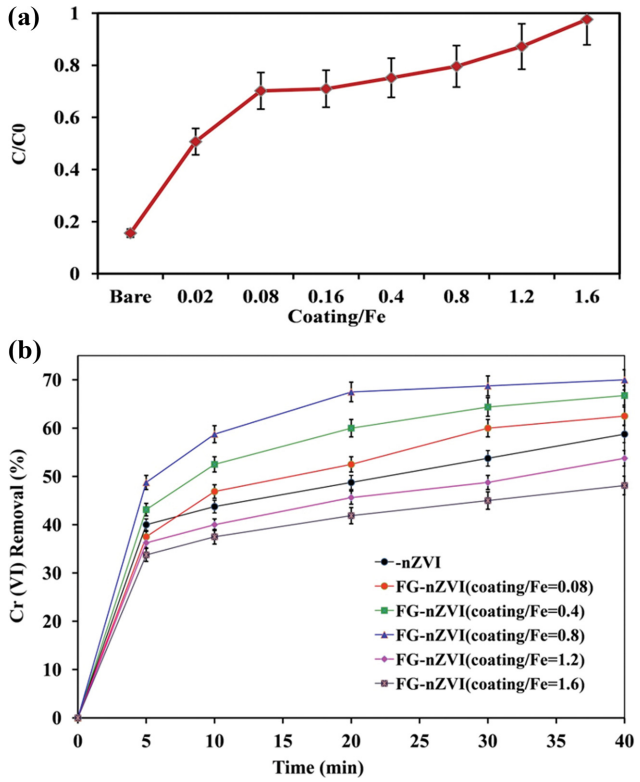



**Fig. 2. Effect of Coating/Fe ratio on sedimentation of FG-nZVI (a), Cr(VI) removal by FG-nZVI under various mass ratio of Coating/Fe (b) (Cr(VI)=10 mgL$^{-1}$, FG-nZVI=3 mg, pH=7.0, time=40 min).**

ity and aggregation of synthetic FG-nZVI with bare nZVI, and the results are illustrated in Fig. 2 and Fig. S3. According to Fig. S3(a), the sedimentation of the synthetic bar nZVI particles in the middle and lower parts of the bottle was obvious after standing for 10 min. In fact, bar nZVI particles, quickly losing their stability, were completely precipitated or transformed from nano- to micro-size after less than 10 min, indicating no repulsive electrostatic force within them as well as their strong magnetic property and aggregation tendency. Therefore, in the first few minutes, sedimentation occurs rapidly, and then all particles are precipitated after 30 minutes. Furthermore, the steep slope between samples of no coating and Coating/Fe=0.02 in Fig. 2(a) shows how even a small amount of the coating can change the stability result, indicating that flaxseed gum plays an important role in the formation of a space barrier between nanoparticles and the stabilization of nanoparticles. As slope of the curve increases from 0.02 to 0.08, it has a huge increase trend, but it is slower than the preceding step, indicating that the increase in the coating amount has a significant positive impact on nanoparticle stability. The coating layer will actually create a space barrier between particles, resulting in nanoparticles remaining suspended and improving dispersion in aqueous media and mobility in porous media.

In Fig. S3, by increasing the amount of coating, the particle's stability increased from four days to 21 days. Therefore, the FG-nZVI remained stably suspended in solution for long periods of time, 21 days, without showing clear aggregation or precipitation. The results confirm that, in comparison with nZVIs, the dispersive characteristic of FG-nZVIs was greater due to flaxseed glaze preventing iron particles from aggregation and oxidation, maintaining their potential reactivity. Nevertheless, It is interesting that although the presence of high dose of flaxseed glaze coating could lead to the more stable suspension of nZVI particles, increasing the mass ratio of coating/Fe decreased Cr(VI) reduction (Fig. 2(b)). Based on previous studies, the colloidal stability of nZVI particles is negatively associated with the colloidal stability of nZVI particles [31,50]. Thus, in this case, it should be due to fact that when coating concentration enhanced a certain amount, it limited contact between FG-nZVIs and Cr(VI) ions, slowly reversing the promoted influence on Cr(VI) removal. Consequently, FG-nZVI (Coating/Fe=0.8) was chosen for subsequent experiments. The colloidal stability of nZVI particles did not positively correlate with the reactivity of the nanoparticles.

## 3. Study on the Cr(VI) Removal in Batch Experiments

### 3-1. Box-Behnken Design and Statistical Analysis

A set of designed experiments was carried out in a batch system, and the concentration of residual Cr(VI) was determined. The actual and predicted results of the experimental design matrix are demonstrated in Table S4. Comparison of the observed and predicted data indicates their reasonable agreement. The quadratic model obtained regarding selected factors and using BBD is shown in Eq. (6), in which the Cr(VI) residual concentration is as a function of initial Cr(VI) concentration (A), FG-nZVI dosage (B), and pH (C).

$$\text{Residual } Cr^{+}\ (\%) = 6.3599 - (0.9499\times A) + (0.0397\times B) - (1.1388\times C) - (0.0069\times A\times B) + (0.0795\times A\times C) - (0.00774\times B\times C) + (0.0646\times A^2) + (0.0002\times B^2) + (0.0713\times C^2) \quad (6)$$

Analysis of variance (ANOVA), Table S5, was used to determine the model validation and the importance of variables. The p-value less than 0.05 indicated that the results were considered statistically significant. The lack of fit of the model was 0.1589, which indicated the lack of fit was not significant compared to pure error, and also it assured the significantly good model fitting to experimental results in this study. Moreover, the model had an F-value of 178.35, showing that the designed experiments provided sufficient evidence to conclude that the model was significant. The model also presented that the predicted $R^2$ of 0.9483 was reasonable with the adjusted $R^2$ of 0.9895 because their difference was less than 0.1. Therefore, the proposed model can be used for the prediction of Cr(VI) residual concentration.

### 3-2. Model Diagnostics

In Fig. 3, diagnostic plots for the Cr(VI) residual concentration were supplied with Design-Expert software to ensure the best fit of the present model to observed data as outcomes of a set of experiments and expected data. The normal distribution of data can be analyzed by clustering the points around a straight line. If the normal distribution of the residuals, which is computed by the difference between the prediction values of the responses and the actual values, shows a linear pattern, the model is considered reasonable and correct. Fig. 3(a) demonstrates that there was a normal distribution between the results. The scatter plot of the predicted values versus the actual values is used to investigate the absence of

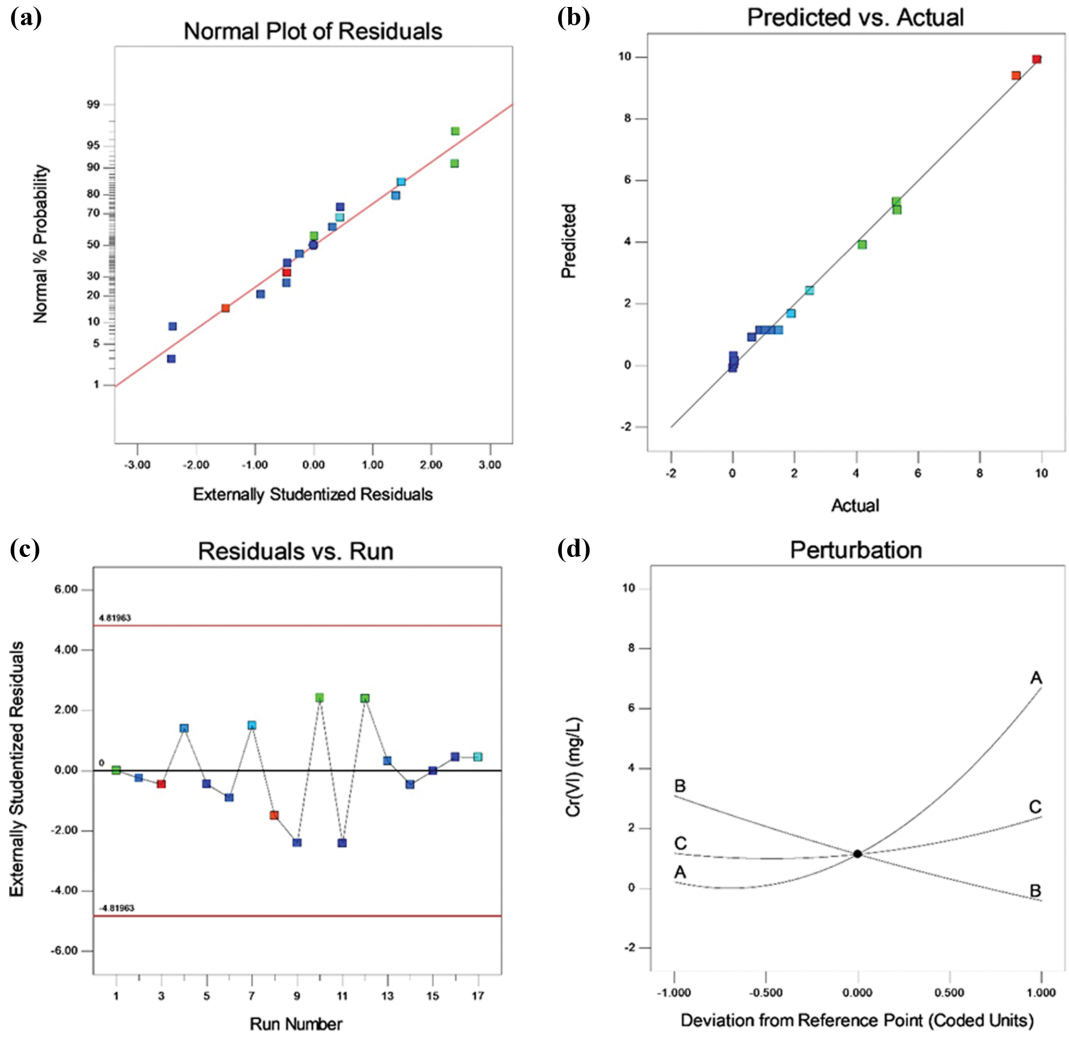



**Fig. 3. Diagnostic plots the Cr(VI) residual concentration (a), (b), (c), and perturbation plots for the Cr(VI) residual concentration (d).**

constant error and exhibit the data in good agreement with those predicted by the model. According to Fig. 3(b), the points located within limits, and consequently, the predicted values had an excellent agreement with experimental results. Fig. 3(c) represents the residual against the order of runs which is a particular type of scatter plot. It describes that the points were randomly scattered in the plot, which means no lurking variables have affected the response during the experiment and the model was consistent with the observed data.

3-3. A Comparative Study on the Effects of Variables

The influence of three factors was compared by the perturbation plot (Fig. 3(d)). The perturbation plot helps to determine which factors have a more significant impact on the target response. It is evident that all operating parameters had significant effects on the Cr(VI) residual concentration; nonetheless, the initial concentration of Cr(VI) revealed the most significant impact on the Cr(VI) residual concentration than the other factors owing to having a steep slope. This may be related to the increase in the concentration of Cr(VI) resulting in the formation of a thin passivating film on the outer surfaces of nZVI, significantly restricting the number of transferring electrons from iron core to Cr(VI), and as a consequence, reducing the rate of Cr(VI) reduction [11,53-55].

Conversely, pH had less influence because its line was relatively flat. However, a slight increase in Cr(VI) residual concentration was observed by increasing in pH. Results from this investigation agree with reports in the previous findings that have confirmed the decrease in the removal rate of Cr(VI) results from the increase in the initial solution pH. It can be postulated that, at high pH values, a mixed Fe and Cr oxyhydroxides is created on the nZVI surface [56-58].

The perturbation plot (Fig. 3(d)) also showed that the increase in the Cr(VI) initial concentration had a negative influence and resulted in the increase in the Cr(VI) residual concentration, while a decrease in the Cr(VI) residual concentration was observed when FG-nZVI dosages increased. This may be due to the reduction reaction of Cr(VI) with nZVI on the surface of iron, and therefore, increasing nZVI concentration results in enhancing reactive sites and making an excellent removal capacity of Cr(VI) [55].

3-4. Effect of Variables and their Interactions

Response surface plots were generated from Eq. (6) to under-

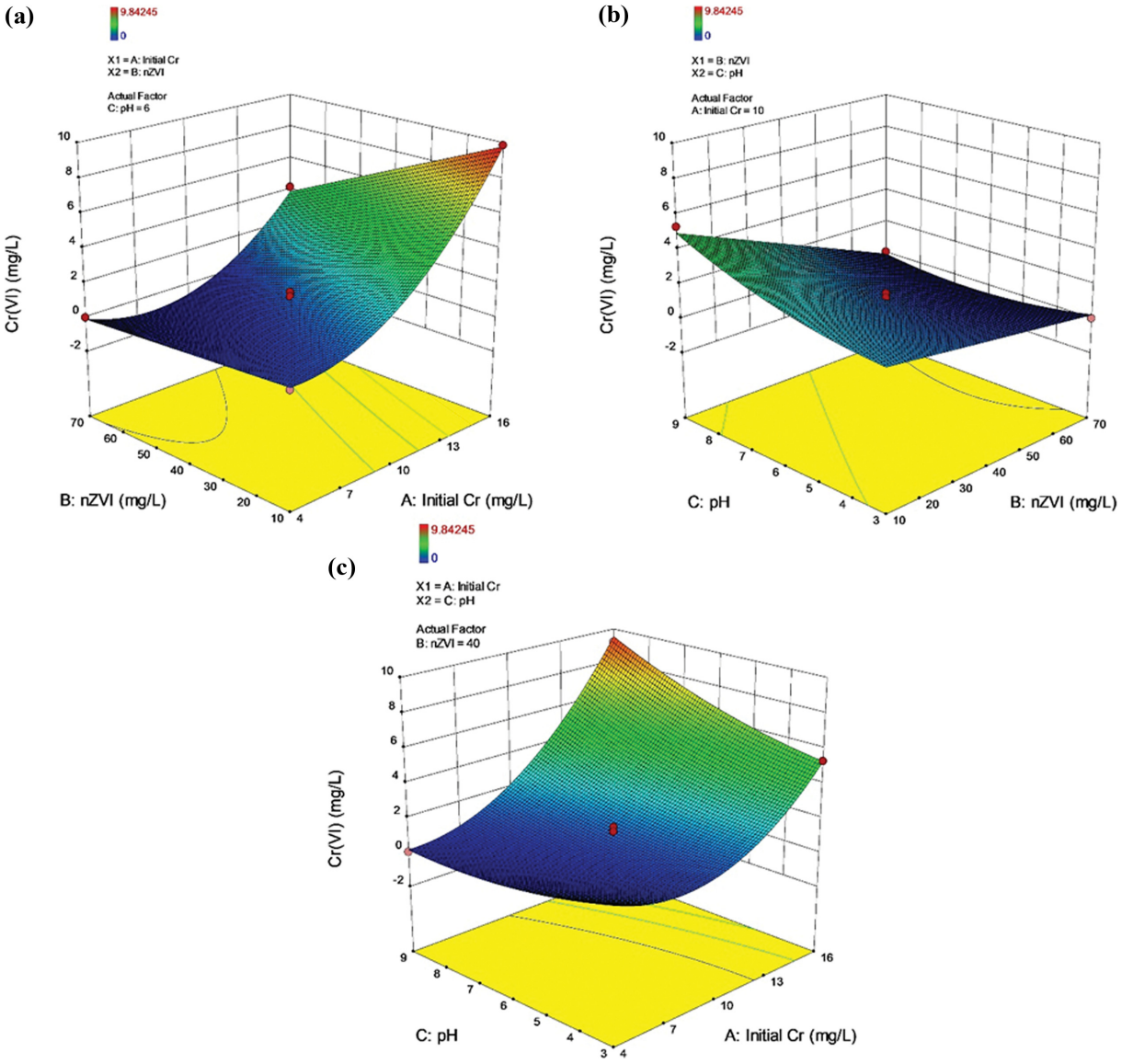



**Fig. 4. Interactive effect of Cr(VI) initial concentration and FG-nZVI dosage on the Cr(VI) residual concentration (a), interactive effect of pH and FG-nZVI dosage on the Cr(VI) residual concentration (b), and interactive effect of pH and Cr(VI) initial concentration on the Cr(VI) residual concentration (c).**

stand the impact of the three variables on the Cr(VI) residual concentration and the relationships between the variables. Fig. 4(a) shows the interaction between the Cr(VI) initial concentration and the FG-nZVI dosage on the Cr(VI) residual concentration at the pH of 6. The results in Fig. 4(a) show that the Cr(VI) residual level increased by increasing the initial Cr(VI) concentration and decreasing the FG-nZVI dosage. The reason may be that, at a fixed amount of FG-nZVI, the available sites stay the same. Therefore, with increasing Cr(VI) concentration, the limit reduction activity causes Cr(VI) removal at a low efficiency. At the Cr(VI) initial concentration of 4 mg $L^{-1}$, Cr(VI) was removed entirely at almost all dosages of FG-nZVI. As can be seen in the results (Fig. 4(b)-(c)), the pH increasing from 3.0 to 9.0 had a little influence on the Cr(VI) removal by FG-nZVI, which can be due to flaxseed glaze, used as a coating. This coating can effectively protect the surface charge of nanoparticles and the electrostatic interaction between nanoparticles and Cr(VI) ions against being affected by a wide pH range. Furthermore, it protects the nZVI surface from the formation of an oxide layer (the Fe-Cr passivation layer) that can occur at different pH levels, except at a low enough pH to dissolve it [59]. Thus, the removal of Cr(VI) can take place under acidic, neutral, and alkaline conditions. As indicated in Fig. 4(b), pH and initial concentration of Cr(VI) had little interaction with each other. At high levels of pH, the Cr(VI) residual concentration increased rapidly by increasing the Cr(VI) initial concentration, indicating the active sites of the certain dose of nZVI particles were inevitably saturated with increasing initial Cr(VI) concentration. The effect of pH and the FG-nZVI dosage on Cr(VI) removal is also illustrated in Fig. 4(c). The results showed that increasing pH and the FG-nZVI dosage gradually decreased the Cr(VI) residual con-

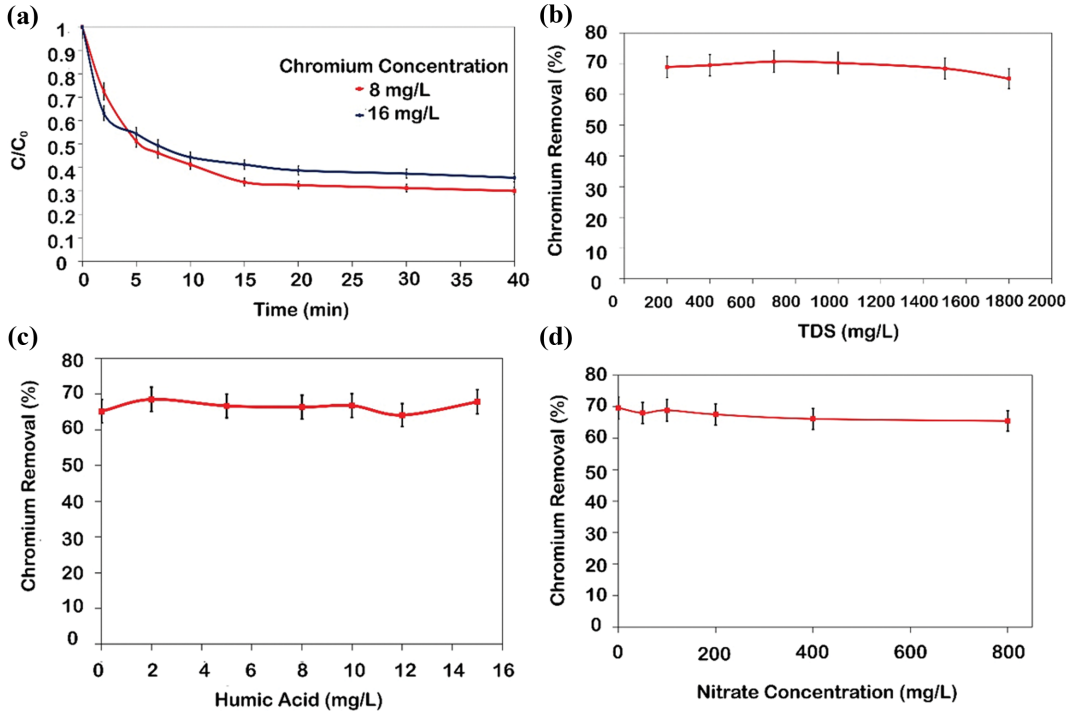



**Fig. 5. The effect of time (Cr(VI)=8 & 16 mgL$^{-1}$, FG-nZVI=3 & 6 mg, pH=7.0) (a), TDS (Cr(VI)=10 mgL$^{-1}$, FG-nZVI=3 mg, TDS=200 to 1,800 mgL$^{-1}$, pH=7.0, Time=40 min) (b), HA (Cr(VI)=10 mgL$^{-1}$, FG-nZVI=3 mg, HA=2 to 15 mgL$^{-1}$, pH=7.0, Time=40 min) (c), and nitrate (Cr(VI)=10 mgL$^{-1}$, FG-nZVI=3 mg, $NO_3^-$=0 to 800 mgL$^{-1}$, pH=7.0, Time=40 min) (d) on the Cr(VI) removal.**

centration. The higher dosage of FG-nZVI might enhance the reduction of Cr(VI) by increasing the surface area for reaction, which can result from less aggregation and settling of nZVI due to the stabilizing influence of flaxseed glaze.

3-5. Optimization of Variable Values

The optimization for FG-nZVI dosage based on reducing Cr(VI) contamination level for drinking water was performed by utilizing Design Expert 10 software. The maximum permissible limit of Cr(VI) in drinking has been set at 0.05 mg L$^{-1}$ by different organizations like the World Health Organization (WHO), U.S. Environmental Protection Agency (US-EPA), and European Environmental Agency (EU) [40]. The optimal amount of FG-nZVI was evaluated at 62.73 mg L$^{-1}$ when applying 4 mg L$^{-1}$ at the optimum pH 6.64 and the initial Cr(VI) residual concentrations of 0.05 mg L$^{-1}$.

3-6. Effect of Time

Due to the high reactivity of FG-nZVI, the influence of time on Cr(VI) reduction was investigated, ranging from 0 to 40 min. For this purpose, two series of similar experiments were conducted in two different Cr(VI) concentrations (8 and 16 mg L$^{-1}$), two different FG-nZVI dosages (3 and 6 mg), and pH=7.0. After the reaction time, all samples were aerated with an aquarium pump to stop the reaction and settle down the iron in the solution. As presented in Fig. 5(a), high removal of Cr(VI) occurred during the first min of the reaction due to the high reactivity of FG-nZVI, and the removal reaction stopped after 15 min because of the total consumption of nZVI.

3-7. Effect of TDS

According to prior studies, the presence of cations influenced the stability of nZVI particles and led to more aggregation of nZVI particles due to larger particle size and decreased specific surface area. In addition, the existence of cations impacted the speciation of pollutants by creating complexes, precipitating, or directly competing with target metal cations. Moreover, high concentrations of some anions such as $HCO_3^-$ and $CO_3^{2-}$, and $PO_4^{3-}$ had an essential inhibitory effect on the Cr(VI) removal. In contrast, the removal of Cr(VI) was promoted by high concentrations of $SO_4^{2-}$ and $NO_3^-$ [11,32,60]. In this study, the removal of Cr(VI) in the presence of TDS was examined (Fig. 5(b)). This was achieved by preparing a synthetic solution containing TDS at a concentration of 2,000 mg L$^{-1}$. Table 1 illustrates the TDS composition of the prepared solution. The removal of Cr(VI) was investigated in the presence of 200 to 1,800 mg L$^{-1}$ TDS (Fig. 5(b)). These experiments were conducted in the Cr(VI) concentration of 10 mg L$^{-1}$, FG-nZVI dosage of 3 mg, the TDS concentration range between 200 to 1,800 mg L$^{-1}$, pH of 7.0, and the reaction time of 40 min. According to Fig. 5(b), the amount of Cr(VI) removal was not significantly affected by the increase in TDS, and the rate of Cr(VI) removal was lower than 70% at the TDS concentration of 2,000 mg L$^{-1}$. On the whole, TDS had no significant effect on the removal of Cr(VI) by FG-nZVIs, which means that FG-nZVIs are well-suited for removing

**Table 1. The TDS composition and concentration of 2,000 mg L$^{-1}$**

| Cation | mg L$^{-1}$ | Anion | mg L$^{-1}$ |
|---|---|---|---|
| $Mg^{2+}$ | 99 | $SO_4^{2-}$ | 392.4 |
| $Ca^{2+}$ | 236.7 | $Cl^-$ | 420.1 |
| $Na^+$ | 158 | $HCO_3^-$ | 419.3 |
| $K^+$ | 106 | $NO_3^-$ | 168.5 |

Cr(VI) from groundwater with high TDS.

3-8. Effect of HA

Based on previous reports, carboxylic and phenolic groups in humic acid (HA) occupy active sites on the nZVI surface due to a complex chemical reaction. These new strong bands act as a barrier to electron transfer between the nZVI and the contaminants. Moreover, the inhibitory effect of HA was associated with the competition between adsorbed HA and target pollutants for reactive sites. Therefore, the influence of HA on the removal of Cr(VI) by FG-nZVI should be taken into account. These experiments were conducted in the Cr(VI) concentration of 10 mg $L^{-1}$, the HA concentration range between 2 to 15 mg $L^{-1}$, FG-nZVI dosage of 3 mg, pH of 7.0, and the reaction time of 40 min (Fig. 5(c)). As demonstrated in Fig. 5(c), the Cr(VI) removal was approximately equal for different concentrations of HA. It means that the increase in HA concentration, classified as an organic material, had no substantial impact on the removal of Cr(VI) by FG-nZVIs. This is most likely due to flaxseed glaze, which protected the nZVI from the reaction with HA and decreased competition between the adsorbed HA and Cr(VI) [34,57,61,62].

3-9. Effect of $NO_3^-$

Groundwater contains many different ions, particularly $NO_3^-$ which is considered one of the major environmental concerns in nitrogen-fertilized areas. Based on previous studies, $NO_3^-$ resulted in the formation of film coatings from $Fe^0$ reduction, which inhibited reactions. Thus, the removal rate of Cr(VI) in the presence of $NO_3^-$ was investigated at the Cr(VI) concentration of 10 mg $L^{-1}$, various $NO_3^-$ concentrations (0-800 mg $L^{-1}$), FG-nZVI dosage of 3 mg, pH of 7.0, and the reaction time of 40 min (Fig. 5(d)). As shown in Fig. 5(d), although nZVIs react with $NO_3^-$ and are also used to remove nitrate from groundwater, they had no effect on removing Cr(VI). This is because Cr(VI) is more reactive than $NO_3^-$ and nZVIs selectively react with Cr(VI). The results of this study are consistent with previous findings, which indicated that the increase in $NO_3^-$ concentrations did not affect the final removal rate of Cr(VI) by CMC-nZVI [63]. As a result, the initial nitrate concentration in the solutions was present without a decrease in concentration at the end of the reaction.

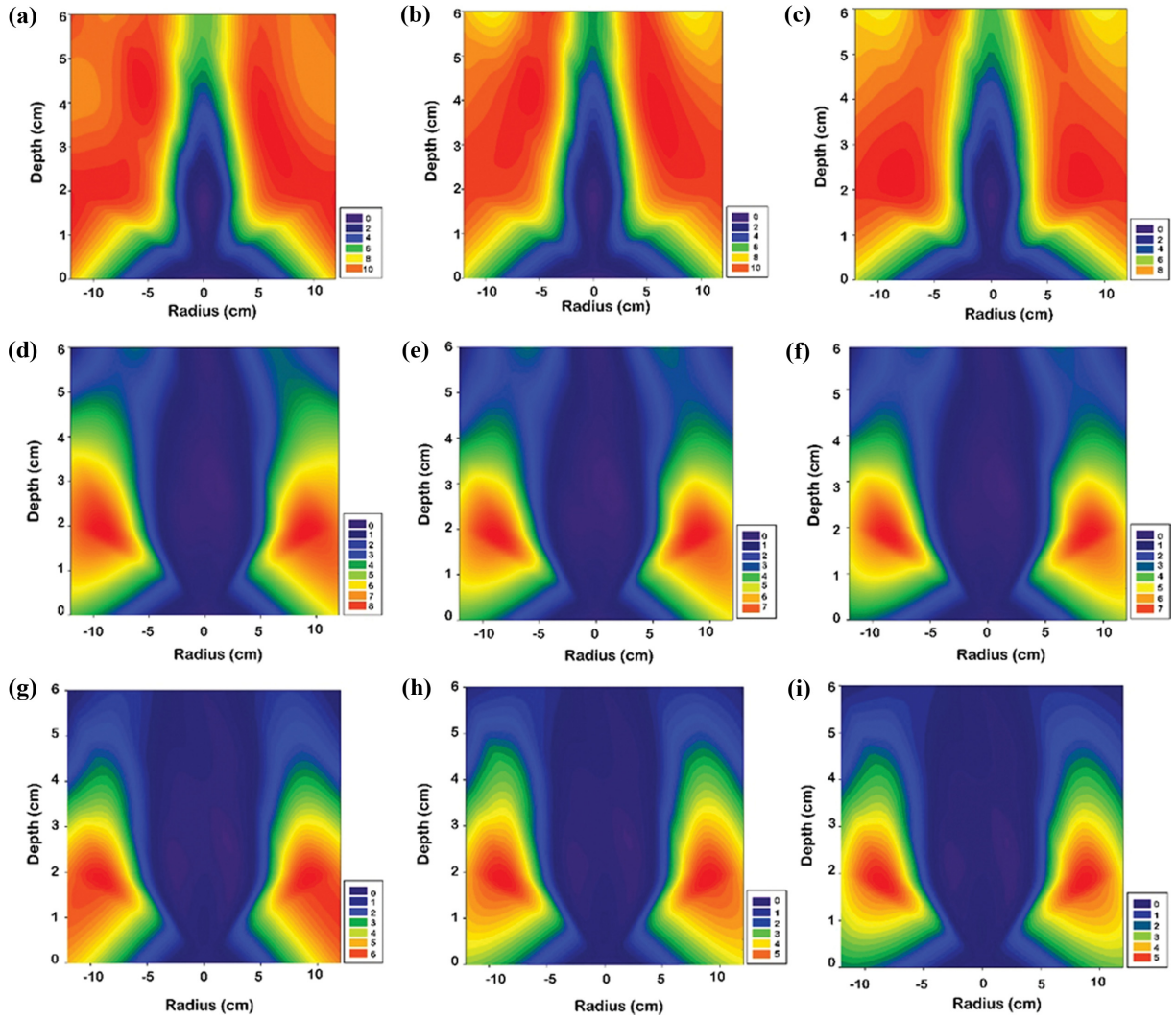



**Fig. 6. Contour plots of the Cr(VI) removal in a saturated media for 0.05 mg $L^{-1}$ FG-nZVIs, 12 mg $L^{-1}$ Cr(VI) initial concentration, the injection background solution of 0, 30, and 60 mLmin$^{-1}$ after 5, 20, and 60 min reaction time (a)-(c), (d)-(f), and (g)-(i), respectively.**

## 4. Cr(VI) Removal in a Saturated Porous Medium

### 4-1. Effect of Injection Background Solution on FG-nZVI Deposition and Transport

The background solution was injected to investigate the mobility of dispersed FG-nZVIs in water-saturated porous media. According to the results (Fig. 6), the injection background solution was significantly effective in transporting FG-nZVIs in porous media. It revealed a diversity of Cr(VI) reduction patterns, as shown in Fig. 6(a)-(c), that FG-nZVI particles had minimal mobility when the flow rate of injection background solution was zero. This indicates that injected nanoparticles remained near the injection point, resulting in the zero residual concentration of Cr(VI) around the injection point. However, the residual concentration of Cr(VI) increased rapidly with increased radius and depth from the injection point due to the accumulation of nanoparticles in the injection point. The blue areas indicate the lowest measured values of Cr(VI) residual concentration in these figures, and red and orange areas indicate areas with high Cr(VI) residual concentration. According to the results of increasing the flow rate of the background solution to 30 and 60 mL $min^{-1}$ (Fig. 6(d)-(i)), nanoparticles had better mobility (Fig. S4), and Cr(VI) residual concentrations decreased significantly at the same experimental conditions due to widely distributed FG-nZVI particles. According to contour plots (Fig. 6(d)-(i)), Cr(VI) residual concentration decreased with increasing depth. In addition, the Cr(VI) reduction patterns illustrate that the Cr(VI) residual concentrations are enhanced in the middle depths of porous media and at a farther radius from the injection point. It can result from injection pressure in the porous media, limiting the mobility of nZVI particles in the subsurface zones, especially at farther radius (Fig. S5).

### 4-2. Effect of Time

This research investigated the effect of time on the Cr(VI) removal with FG-nZVIs in a saturated porous media by collecting the samples at three various times (5, 20, and 60 min) in the same experimental conditions. The results of the first three experiments in Table S2 are depicted in Fig. 6. According to the results, enhancing the time has less effect on the efficiency of Cr(VI) reduction, and as a result, there was no significant change in residual concentrations of Cr(VI) after 5 min up to 60 min. Consequently, the results from saturated porous media were in agreement with reports in the effect of time in batch experiments (3.2.6) that the time was not a major factor affecting the concentrations of residual Cr(VI) due to the high reactivity of FG-nZVIs with Cr(VI) during the first 5 minutes of the reaction (Fig. S5).

### 4-3. Effect of Initial Cr(VI) Concentration

To understand the impact of initial Cr(VI) concentration in a saturated porous media, the Cr(VI) initial concentration of 6 mg $L^{-1}$ in experiment 4 was compared with experiment 3 in Table S2. In these experiments, the FG-nZVI concentration and the flow rate of the injection background solution were kept constant at 0.05 mg $L^{-1}$ and 60 mL $min^{-1}$, respectively. As observed in Fig. 7(a)-(f), initial Cr(VI) concentration considerably influenced the reductive removal of Cr(VI) via FG-nZVI particles. The experiment results exhibit lower removal efficiency of Cr(VI) in saturated porous media when the initial Cr(VI) concentration increased from 7 mg $L^{-1}$ to 0.35 mg $L^{-1}$ in the same experimental condition, which is in agreement with previous reports of an investigation into nZVI particles (Fig. S6) [55,64,65].

### 4-4. Effect of FG-nZVI Dosages

The impact of FG-nZVI dosage on the Cr(VI) removal in a sat-

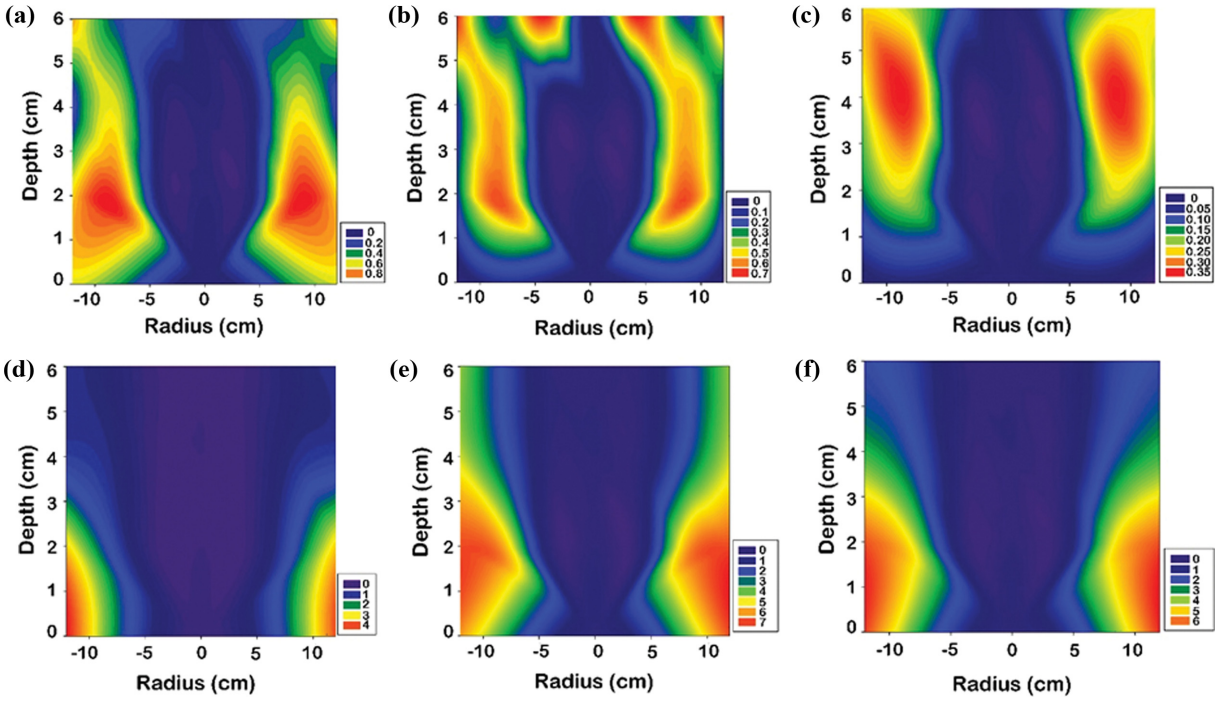



**Fig. 7. Contour plots of the Cr(VI) removal in a saturated media for 0.05 mg $L^{-1}$ FG-nZVIs, 60 mL$min^{-1}$ injection background solution of, the Cr(VI) initial concentration of 6 and 12 mg $L^{-1}$, after 5, 20, and 60 min reaction time (a)-(c) and (d)-(f), respectively.**

urated porous media was determined by comparing the results of experiment 3 with experiment 5. In these experiments, the nZVI was performed in various dosages (0.05 and 0.075 mg $L^{-1}$). The other constant experimental variables were 12 mg $L^{-1}$ of initial Cr(VI) concentration and the second injection flow rate of 60 mL$min^{-1}$ at the same time. Fig. 7(a)-(f) show the three-dimensional response surface and contour plots of the Cr(VI) residual concentration when the number of nanoparticles was 50 percent less than experiment 3 (0.075<0.05 mg $L^{-1}$). As the FG-nZVI dosage increased from 0.075 mg $L^{-1}$ to 0.05 mg $L^{-1}$, the Cr(VI) residual concentration increased significantly from 5 mg $L^{-1}$ to 0.5 mg $L^{-1}$. Thus, according to the results, the Cr(VI) residual concentrations decreased 10 times with the increase in FG-nZVI dosage from 0.075 mg $L^{-1}$ to 0.05 mg $L^{-1}$, considering the significant influence of FG-nZVI dosage on removal of Cr(VI) (Fig. S6).

## SOME HIGHLIGHTS ON LIMITATIONS AND THE FUTURE PROSPECTS

There are a few concerns that need to be addressed for iron nanoparticles and their organic coating. Although iron nanoparticles are popular as a research subject, nZVIs adversely influence microorganisms, animal cells, plant cells, and human cells. This explains why a remediation process must be performed under controlled conditions, which takes all necessary precautions to keep nZVIs from migrating outside of the area remediated [66]. Although the toxicity of nZVI is presumably low due to its being a common element in soil and an essential element for the growth of all organisms, determining how toxic it is can be quite challenging since it is affected not just by its physicochemical properties but also by the test organism species, its dose, and environmental conditions [67]. Hence, an in-depth analysis of all the potential factors that may impact nZVI's toxicity is necessary in order to fully understand its toxicity. On the other hand, it is important to note that by applying a suitable modification, an appropriate method of synthesis, or an appropriately selected dose, nZVI's negative impact on the environment can be significantly reduced [68]. The second case involves flaxseed glaze, which is an environmentally friendly material that can be degraded by microorganisms. Thus, flaxseed glaze can reduce the stability of nZVI particles in aqueous suspensions and aggregate them because of its biodegradability. FG-nZVI's stability in aqueous environments should be tested for its effects on biodegradation in the environment.

## CONCLUSION

FG-nZVIs were successfully synthesized by using a novel continuous synthesis system and flaxseed glaze for surface coating as a natural stabilizer with extremely high performance for stabilizing nanoparticles. FE-SEM images and DLS analyses of synthesized nZVI particles indicate that the particles were spherical and less than 100 nm in size, and in addition, they have a narrow and uniform size distribution. The stability and dispersibility of iron nanoparticles were significantly improved by increasing the coating/Fe ratio from 0 to 1.6, resulting in less sedimentation and greater particle stability (10 min to 21 days). In aqueous and saturated porous media, FG-nZVI displayed excellent Cr(VI) removal (almost complete removal). The results illustrate that pH, TDS, HA, and $NO_3^-$ have minimal impacts on the final Cr(VI) removal in aqueous. In saturated porous media, the injection background solution had a great effect on increasing nanoparticle transmission, resulting in appropriate removal in the required radius. Therefore, the synthesized FG-nZVI is a promising low-cost material for effective in-situ remediation of Cr(VI)-contaminated both acidic and alkaline soils and water.

## ACKNOWLEDGEMENT

The authors would like to express their gratitude to the Nanotechnology Research Center of the School of the Environment, College of Engineering, University of Tehran.

## SUPPORTING INFORMATION

Additional information as noted in the text. This information is available via the Internet at http://www.springer.com/chemistry/journal/11814.

## REFERENCES

1. S. Chandra, L. K. S. Chauhan, P. N. Pande and S. K. Gupta, *Environ. Toxicol.*, **19**, 129 (2004).
2. G. T. Rao, V. V. S. G. Rao, K. Ranganathan, L. Surinaidu, J. Mahesh and G. Ramesh, *Hydrogeol. J.*, **19**, 1587 (2011).
3. J. Zhang, X. Zhang, T. Zhou, Y. Huang and L. Zhao, *J. Clean. Prod.*, **315**, 128219 (2021).
4. S. N. Malik, S. M. Khan, P. C. Ghosh, A. N. Vaidya, G. Kanade and S. N. Mudliar, *Sci. Total Environ.*, **678**, 114 (2019).
5. Q. Yu, J. Guo, Y. Muhammad, Q. Li, Z. Lu, J. Yun and Y. Liang, *J. Environ. Manage.*, **276**, 111245 (2020).
6. D. Blowes, *Science* (80-. ). **295**, 2024 (2002).
7. R. Fu, X. Zhang, Z. Xu, X. Guo, D. Bi and W. Zhang, *Sep. Purif. Technol.*, **174**, 362 (2017).
8. I. Maamoun, O. Eljamal, O. Falyouna, R. Eljamal and Y. Sugihara, *Ecotoxicol. Environ. Saf.*, **200**, 110773 (2020).
9. I. Maamoun, O. Falyouna, R. Eljamal, K. Bensaida and O. Eljamal, *Int. J. Environ. Sci. Dev.*, **12**, 131 (2021).
10. P. Liu, X. Wang, J. Ma, H. Liu and P. Ning, *Chemosphere*, **220**, 1003 (2019).
11. J. Li, M. Fan, M. Li and X. Liu, *Sci. Total Environ.*, **717**, 137112 (2020).
12. H. Peng and J. Guo, *Environ. Chem. Lett.*, **18**, 2055 (2020).
13. A. R. Esfahani, A. F. Firouzi, G. Sayyad and A. R. Kiasat, *J. Ind. Eng. Chem.*, **20**, 2671 (2014).
14. M. Velimirovic, D. Schmid, S. Wagner, V. Micić, F. von der Kammer and T. Hofmann, *Sci. Total Environ.*, **563-564**, 713 (2016).
15. R. Xing, W. Wang, T. Jiao, K. Ma, Q. Zhang, W. Hong, H. Qiu, J. Zhou, L. Zhang and Q. Peng, *ACS Sustain. Chem. Eng.*, **5**, 4948 (2017).
16. R. Guo, T. Jiao, R. Li, Y. Chen, W. Guo, L. Zhang, J. Zhou, Q. Zhang and Q. Peng, *ACS Sustain. Chem. Eng.*, **6**, 1279 (2018).
17. R. Xing, W. Wang, T. Jiao, K. Ma, Q. Zhang, W. Hong, H. Qiu, J.

Zhou, L. Zhang and Q. Peng, *ACS Sustain. Chem. Eng.*, **5**, 4948 (2017).
18. H. Dong, Y. Xie, G. Zeng, L. Tang, J. Liang, Q. He, F. Zhao, Y. Zeng and Y. Wu, *Chemosphere*, **144**, 1682 (2016).
19. A. V. B. Reddy, Z. Yusop, J. Jaafar, Y. V. M. Reddy, A. Bin Aris, Z. A. Majid, J. Talib and G. Madhavi, *J. Environ. Chem. Eng.*, **4**, 3537 (2016).
20. H. Dong, Y. Zeng, G. Zeng, D. Huang, J. Liang, F. Zhao, Q. He, Y. Xie and Y. Wu, *Sep. Purif. Technol.*, **165**, 86 (2016).
21. C. Jiao, Y. Cheng, W. Fan and J. Li, *Int. J. Environ. Sci. Technol.*, **12**, 1603 (2015).
22. Z. Li, S. Xu, G. Xiao, L. Qian and Y. Song, *J. Environ. Manage.*, **244**, 33 (2019).
23. X. Lv, X. Xue, G. Jiang, D. Wu, T. Sheng, H. Zhou and X. Xu, *J. Colloid Interface Sci.*, **417**, 51 (2014).
24. W. Liu, J. Bai, Z. Chi, L. Ren and J. Dong, *J. Environ. Chem. Eng.*, **9**, 104987 (2021).
25. R. Li, H. Dong, R. Tian, J. Chen and Q. Xie, *Sep. Purif. Technol.*, **250**, 117230 (2020).
26. J. Deng, H. Dong, L. Li, Y. Wang, Q. Ning, B. Wang and G. Zeng, *Sep. Purif. Technol.*, **227**, 115731 (2019).
27. J. Liu, A. Liu and W.-x. Zhang, *Chem. Eng. J.*, **303**, 268 (2016).
28. I. Maamoun, O. Eljamal, O. Falyouna, R. Eljamal and Y. Sugihara, *Water Sci. Technol.*, **80**, 1996 (2019).
29. I. Maamoun, R. Eljamal, O. Falyouna, K. Bensaida, Y. Sugihara and O. Eljamal, *J. Mol. Liq.*, **328**, 115402 (2021).
30. O. Falyouna, I. Maamoun, K. Bensaida, A. Tahara, Y. Sugihara and O. Eljamal, *J. Colloid Interface Sci.*, **605**, 813 (2022).
31. J. F. Gao, H. Y. Li, K. L. Pan and C. Y. Si, *RSC Adv.* (2016).
32. X. Zhao, W. Liu, Z. Cai, B. Han, T. Qian and D. Zhao, *Water Res.*, **100**, 245 (2016).
33. S. Bhattacharjee, M. Basnet, N. Tufenkji and S. Ghoshal, *Environ. Sci. Technol.*, **50**, 1812 (2016).
34. H. Dong, Q. He, G. Zeng, L. Tang, C. Zhang, Y. Xie, Y. Zeng, F. Zhao and Y. Wu, *J. Colloid Interface Sci.*, **471**, 7 (2016).
35. H. Dong, Y. Cheng, Y. Lu, K. Hou, L. Zhang, L. Li, B. Wang, Y. Wang, Q. Ning and G. Zeng, *Sep. Purif. Technol.*, **210**, 504 (2019).
36. H. Dong, L. Li, Y. Wang, Q. Ning, B. Wang and G. Zeng, *Water Environ. Res.*, **92**, 646 (2020).
37. Y. Cheng, H. Dong, Y. Lu, K. Hou, Y. Wang, Q. Ning, L. Li, B. Wang, L. Zhang and G. Zeng, *Chemosphere*, **220**, 523 (2019).
38. R. Eljamal, O. Eljamal, I. Maamoun, G. Yilma and Y. Sugihara, *J. Mol. Liq.*, **315**, 113714 (2020).
39. J. Adusei-Gyamfi and V. Acha, *RSC Adv.*, **6**, 91025 (2016).
40. Q. Wang, H. Qian, Y. Yang, Z. Zhang, C. Naman and X. Xu, *J. Contam. Hydrol.*, **114**, 35 (2010).
41. M. Stefaniuk, P. Oleszczuk and Y. S. Ok, *Chem. Eng. J.*, **287**, 618 (2016).
42. C. Mystrioti, A. Xenidis and N. Papassiopi, *Desalin. Water Treat.*, **56**, 1162 (2015).
43. Technical/Regulatory Guidance Permeable Reactive Barrier : Technology Update PRB-5 (2011).
44. H. M. Abd El-Aziz, R. S. Farag and S. A. Abdel-Gawad, *Nanotechnol. Environ. Eng.*, **5**, 1 (2020).
45. S. M. Mirbahoush, N. Chaibakhsh and Z. Moradi-Shoeili, *Chemosphere*, **231**, 51 (2019).
46. R. Yadav, A. K. Sharma and J. N. Babu, *J. Environ. Chem. Eng.*, **4**, 681 (2016).
47. P. Anju Rose Puthukkara, T. Sunil Jose and S. Dinoop lal, *Environ. Nanotechnol., Monit. Manag.*, **14**, 100295 (2020).
48. M. H. Dehghani, R. R. Karri, M. Alimohammadi, S. Nazmara, A. Zarei and Z. Saeedi, *J. Mol. Liq.*, **311**, 113317 (2020).
49. S. N. Malik, P. C. Ghosh, A. N. Vaidya and S. N. Mudliar, *J. Hazard. Mater.*, **357**, 363 (2018).
50. K. M. Tripathi, T. S. Tran, Y. J. Kim and T. Y. Kim, *ACS Sustain. Chem. Eng.*, **5**, 3982 (2017).
51. V. V. Thekkae Padil, J. Filip, K. I. Suresh, S. Wacławek and M. Černík, *RSC Adv.*, **6**, 110288 (2016).
52. H. Su, Z. Fang, P. E. Tsang, L. Zheng, W. Cheng, J. Fang and D. Zhao, *J. Hazard. Mater.*, **318**, 533 (2016).
53. H. Song, W. Liu, F. Meng, Q. Yang and N. Guo, *Int. J. Environ. Res. Public Health*, **18**, 5921 (2021).
54. D. Jiang, D. Huang, C. Lai, P. Xu, G. Zeng, J. Wan, L. Tang, H. Dong, B. Huang and T. Hu, *Sci. Total Environ.*, **644**, 1181 (2018).
55. A. Ramazanpour Esfahani and A. Farrokhian Firouzi, *Desalin. Water Treat.*, **57**, 15424 (2016).
56. C. Yang, C. Ge, X. Li, L. Li, B. Wang, A. Lin and W. Yang, *Ecotoxicol. Environ. Saf.*, **208**, 111552 (2021).
57. F. Zhu, S. Ma, T. Liu and X. Deng, *J. Clean. Prod.*, **174**, 184 (2018).
58. Q. Wang, H. Qian, Y. Yang, Z. Zhang, C. Naman and X. Xu, *J. Contam. Hydrol.*, **114**, 35 (2010).
59. Y. Cheng, H. Dong and T. Hao, *Sep. Purif. Technol.*, **257**, 117967 (2021).
60. P. Anju Rose Puthukkara, T. Sunil Jose and S. Dinoop lal, *Environ. Nanotechnol., Monit. Manag.*, **14**, 100295 (2020).
61. Z. Xiao, H. Zhang, Y. Xu, M. Yuan, X. Jing, J. Huang, Q. Li and D. Sun, *Sep. Purif. Technol.*, **147**, 466 (2017).
62. F. Zhu, L. Li, W. Ren, X. Deng and T. Liu, *Environ. Pollut.*, **227**, 444 (2017).
63. Z. Li, S. Xu, G. Xiao, L. Qian and Y. Song, *J. Environ. Manage.*, **244**, 33 (2019).
64. X. Qiu, Z. Fang, X. Yan, F. Gu and F. Jiang, *Chem. Eng. J.*, **193-194**, 358 (2012).
65. J. Yang, S. Wang, N. Xu, Z. Ye, H. Yang and X. Huangfu, *J. Hazard. Mater.*, **419**, 126461 (2021).
66. B. I. Kharisov, H. V. Rasika Dias, O. V. Kharissova, V. Manuel Jiménez-Pérez, B. Olvera Pérez and B. Muñoz Flores, *RSC Adv.*, **2**, 9325 (2012).
67. Y. S. El-Temsah and E. J. Joner, *Chemosphere*, **89**, 76 (2012).
68. R. J. Barnes, C. J. van der Gast, O. Riba, L. E. Lehtovirta, J. I. Prosser, P. J. Dobson and I. P. Thompson, *J. Hazard. Mater.*, **184**, 73 (2010).

# Supporting Information

# The removal of Cr(VI) from aqueous and saturated porous media by nanoscale zero-valent iron stabilized with flaxseed gum extract: Synthesis by continuous flow injection method

**Neman Izadi, Banafsheh Haji Ali, Mohammad Sajjad Shahin, and Majid Baghdadi**†

School of Environment, College of Engineering, University of Tehran, Tehran, Iran
(*Received 30 November 2021 • Revised 13 January 2022 • Accepted 17 January 2022*)

**Table S1. The range of the independent variables was studied**

| Variables | Unit | Levels | | |
|---|---|---|---|---|
| | | −1 | 0 | +1 |
| A: Initial Cr(VI) concentration | mg $L^{-1}$ | 4 | 10 | 16 |
| B: FG-nZVI | mg $L^{-1}$ | 10 | 40 | 70 |
| C: pH | - | 3 | 6 | 9 |

**Table S2. Operating conditions of Cr(VI) removal in a saturated porous medium**

| No. | Initial Cr(VI) (mg $L^{-1}$) | FG-nZVI (g) | FG-nZVI injection flow (mL $min^{-1}$) | Injection background solution (mL $min^{-1}$) | Total volume ($cm^3$) | Cr(VI)-contaminated solution volume ($cm^3$) |
|---|---|---|---|---|---|---|
| 1 | 12 | 0.05 | 15 | 0 | 4,000 | 1,400 |
| 2 | 12 | 0.05 | 15 | 30 | 4,000 | 1,400 |
| 3 | 12 | 0.05 | 15 | 60 | 4,000 | 1,400 |
| 4 | 6 | 0.05 | 15 | 60 | 4,000 | 1,400 |
| 5 | 12 | 0.075 | 15 | 60 | 4,000 | 1,400 |

**Table S3. CHNS results for the flaxseed glaze**

| Sample | %C | %H | %N | %S |
|---|---|---|---|---|
| Flaxseed glaze | 39 | 6.02 | 1.77 | 0.19 |

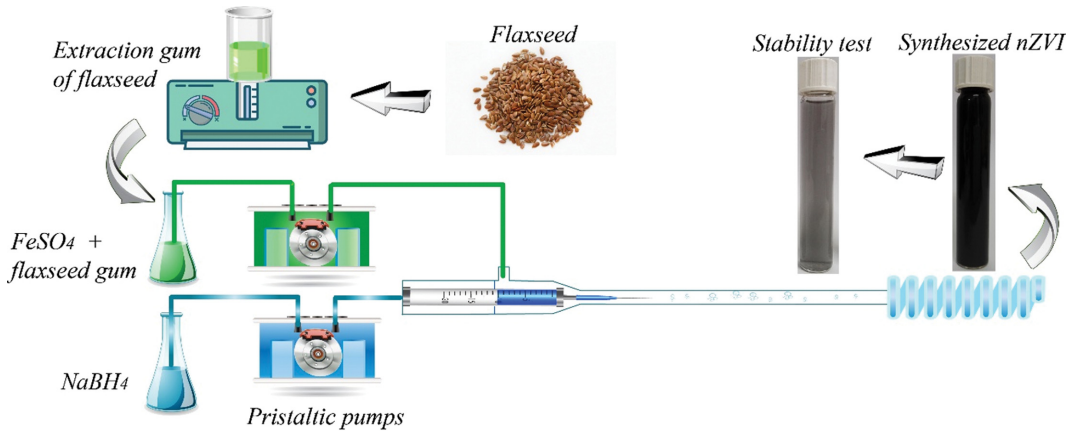



**Fig. S1. FG-nZVI synthesis in the continuous process.**

**Table S4. The experimental design matrix and the observed and predicted values**

| Run | Factors | | | Residual concentration (mg $L^{-1}$) | |
|---|---|---|---|---|---|
| | A: Initial Cr(VI) (mg $L^{-1}$) | B: FG-nZVI (mg $L^{-1}$) | C: pH | Actual | Predicted |
| 1 | 16 | 40 | 3.0 | 5.31 | 5.31 |
| 2 | 10 | 40 | 6.0 | 1.06 | 1.14 |
| 3 | 16 | 10 | 6.0 | 9.84 | 9.72 |
| 4 | 10 | 40 | 6.0 | 1.50 | 1.14 |
| 5 | 10 | 70 | 9.0 | 0.07 | 0.15 |
| 6 | 10 | 40 | 6.0 | 0.88 | 1.14 |
| 7 | 4 | 40 | 3.0 | 1.90 | 1.68 |
| 8 | 16 | 40 | 9.0 | 9.18 | 9.39 |
| 9 | 4 | 10 | 6.0 | 0.63 | 0.91 |
| 10 | 10 | 10 | 9.0 | 5.33 | 5.04 |
| 11 | 10 | 70 | 3.0 | 0.03 | 0.32 |
| 12 | 16 | 70 | 6.0 | 4.20 | 3.91 |
| 13 | 10 | 40 | 6.0 | 1.23 | 1.14 |
| 14 | 10 | 40 | 6.0 | 1.00 | 1.14 |
| 15 | 4 | 40 | 9.0 | 0.03 | 0.03 |
| 16 | 4 | 70 | 6.0 | 0 | 0.01 |
| 17 | 10 | 10 | 3.0 | 2.5 | 2.43 |

**Table S5. ANOVA for the residual concentration model equations of Cr(VI)**

| Factor | SS[a] | dF[b] | MS[c] | F-value | p-Value | |
|---|---|---|---|---|---|---|
| Model | 154.07 | 9 | 17.12 | 175.08 | <0.0001 | Significant |
| A- Initial Cr(VI) | 84.34 | 1 | 84.34 | 862.58 | <0.0001 | |
| B- Nzvi | 24.49 | 1 | 24.49 | 250.44 | <0.0001 | |
| C- Ph | 2.97 | 1 | 2.97 | 30.42 | <0.0009 | |
| AB | 6.30 | 1 | 6.30 | 64.39 | <0.0001 | |
| AC | 8.21 | 1 | 8.21 | 83.95 | <0.0001 | |
| BC | 1.94 | 1 | 1.94 | 19.83 | 0.0030 | |
| $A^2$ | 22.78 | 1 | 22.78 | 233.00 | <0.0001 | |
| $C^2$ | 0.18 | 1 | 0.18 | 1.79 | 0.2225 | |
| Residual | 1.73 | 7 | 1.73 | | | |
| Lack of fit | 0.68 | 3 | 0.098 | 2.58 | 0.1909 | Not significant |
| Pure error | 0.45 | 4 | 0.15 | | | |
| Cor total | 0.23 | 16 | | | | |

$R^2$=0.9956, Adj $R^2$=0.9899, Pred $R^2$=0.9510

[a]Sum of square, [b]Degree of freedom, [c]Mean square

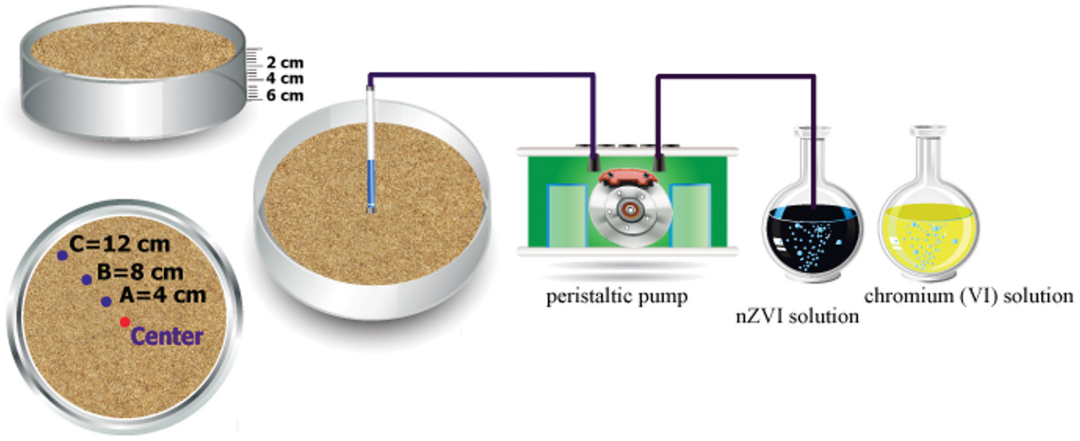



**Fig. S2. The schematic diagram of Column experiments for the removal Cr(VI).**

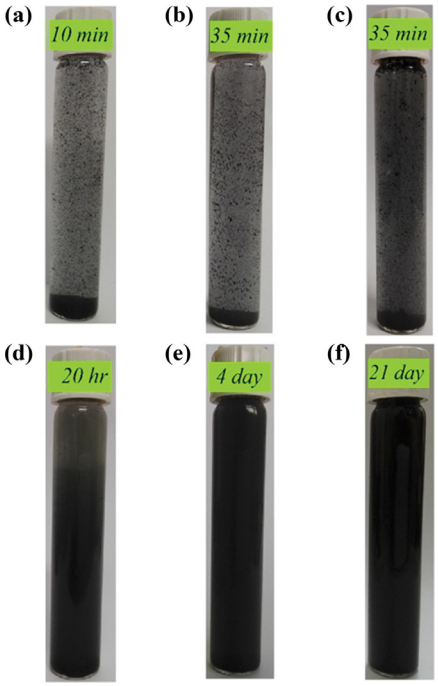



Fig. S3. Sedimentation of synthesized FG-nZVI under different mass ratio of Coating/Fe and bare nZVI, (a) -nZVI, (b) coating/Fe= 0.02, (c) coating/Fe=0.08, (d) coating/Fe=0.4, (e) coating/Fe= 0.8, (f) coating/Fe=1.6.

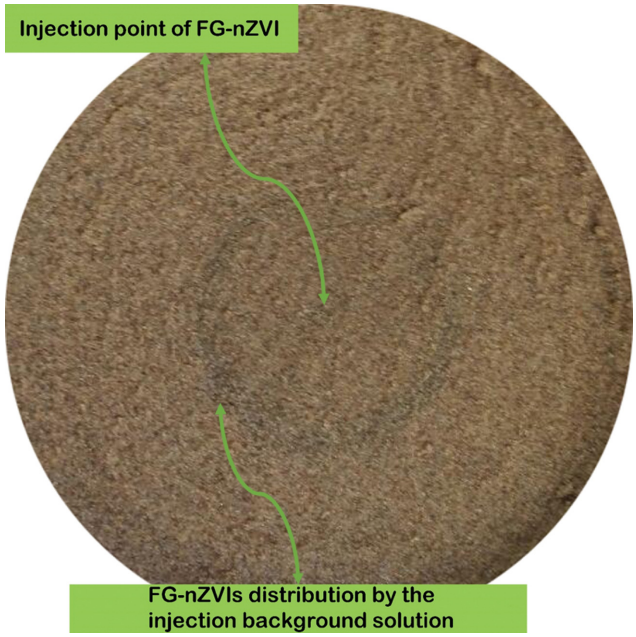



Fig. S4. The injection point and radial distribution of FG-nZVIs around the injection point.

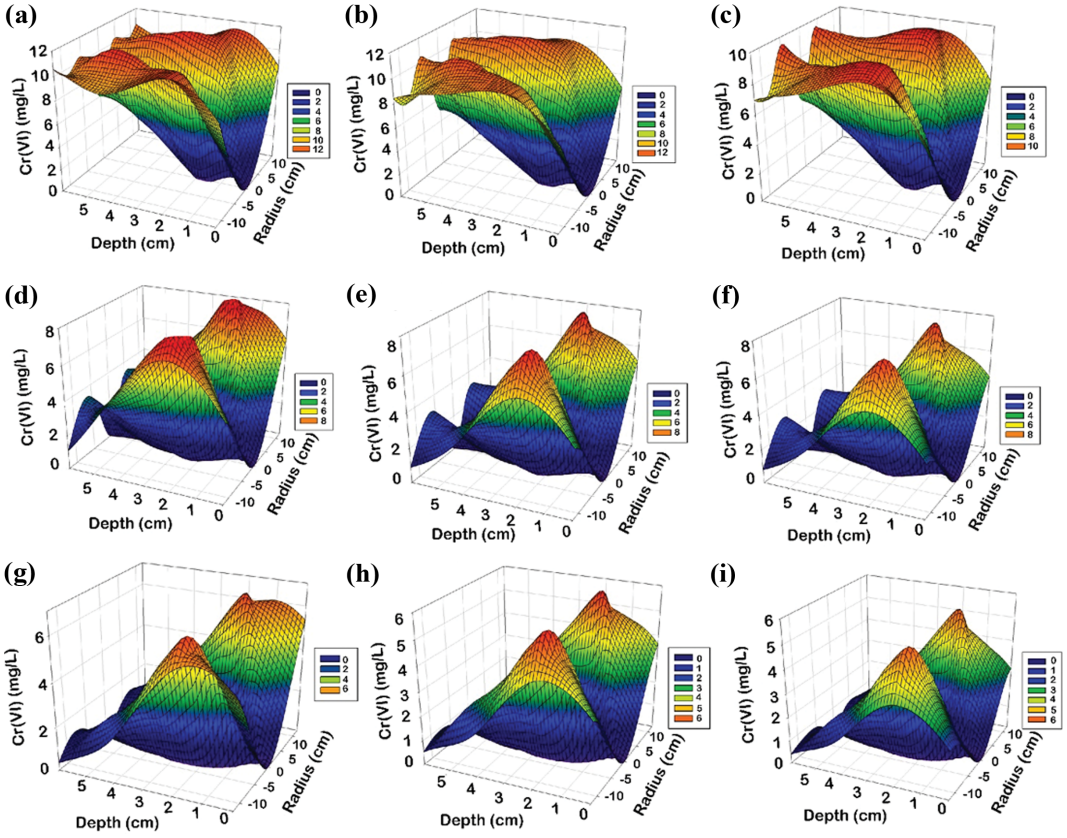



Fig. S5. 3D surfaces of the Cr(VI) removal in a saturated media for 0.05 mg $L^{-1}$ FG-nZVIs, 12 mg $L^{-1}$ Cr(VI) initial concentration, the injection background solution of 0, 30, and 60 mL$min^{-1}$ after 5, 20, and 60 min reaction time (a)-(c), (d)-(f), and (g)-(i), respectively.

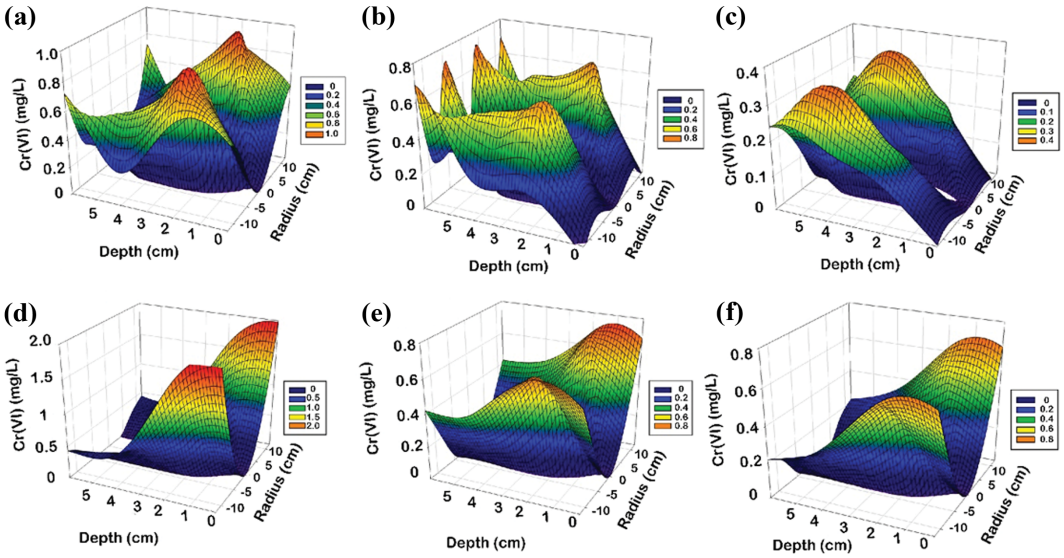



**Fig. S6. 3D surfaces of the Cr(VI) removal in a saturated media for 0.05 mg $L^{-1}$ FG-nZVIs, 60 mL$min^{-1}$ injection background solution of, the Cr(VI) initial concentration of 6 and 12 mg $L^{-1}$, after 5, 20, and 60 min reaction time (a)-(c) and (g)-(i), respectively.**